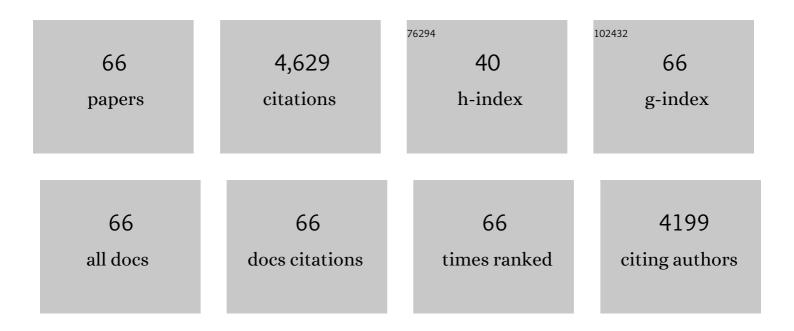


## List of Publications by Year in descending order

Source: https://exaly.com/author-pdf/8118550/publications.pdf Version: 2024-02-01



**GEVILLI** 

#	Article	IF	CITATIONS
1	Gas sensor based on cobalt-doped 3D inverse opal SnO2 for air quality monitoring. Sensors and Actuators B: Chemical, 2022, 350, 130807.	4.0	40
2	Revealing the correlation between gas selectivity and semiconductor energy band structure derived from off-stoichiometric spinel CdGa2O4. Sensors and Actuators B: Chemical, 2022, 352, 131039.	4.0	8
3	Interfacial Stressâ€Modulated Mechanosensitive Upconversion Luminescence of NaErF <sub>4</sub> Based Heteroepitaxial Core–Shell Nanoparticles. Advanced Optical Materials, 2022, 10, 2101702.	3.6	8
4	Bioinspired spike-like double yolk–shell structured TiO <sub>2</sub> @Znln <sub>2</sub> S <sub>4</sub> for efficient photocatalytic CO <sub>2</sub> reduction. Catalysis Science and Technology, 2022, 12, 1092-1099.	2.1	9
5	Mixed potential type YSZ-based NO2 sensors with efficient three-dimensional three-phase boundary processed by electrospinning. Sensors and Actuators B: Chemical, 2022, 354, 131219.	4.0	14
6	A multi-platform sensor for selective and sensitive H2S monitoring: Three-dimensional macroporous ZnO encapsulated by MOFs with small Pt nanoparticles. Journal of Hazardous Materials, 2022, 426, 128075.	6.5	41
7	3-Aminopropyltriethoxysilane functionalized ZnO materials for improving the gas sensitivity to 2-butanone. Sensors and Actuators B: Chemical, 2022, 363, 131845.	4.0	19
8	Photonic Crystal Effects on Upconversion Enhancement of LiErF <sub>4</sub> :0.5%Tm <sup>3+</sup> @LiYF <sub>4</sub> for Noncontact Cholesterol Detection. ACS Applied Materials & Interfaces, 2022, 14, 428-438.	4.0	8
9	Ti <sub>3</sub> C <sub>2</sub> MXene Nanosheets Functionalized with NaErF <sub>4</sub> :0.5%Tm@NaLuF <sub>4</sub> Nanoparticles for Dual-Modal Near-Infrared IIb/Magnetic Resonance Imaging-Guided Tumor Hyperthermia. ACS Applied Nano Materials, 2022, 5, 8142-8153.	2.4	15
10	Highly selective and sensitive optosensing of glutathione based on energy level strongly correlated upconversion nanoprobe. Sensors and Actuators B: Chemical, 2022, 369, 132355.	4.0	1
11	A TPA-DCPP organic semiconductor film-based room temperature NH3 sensor for insight into the sensing properties. Sensors and Actuators B: Chemical, 2021, 327, 128940.	4.0	25
12	Biosensors based on fluorescence carbon nanomaterials for detection of pesticides. TrAC - Trends in Analytical Chemistry, 2021, 134, 116126.	5.8	121
13	Er <sup>3+</sup> self-sensitized nanoprobes with enhanced 1525 nm downshifting emission for NIR-IIb <i>in vivo</i> bio-imaging. Journal of Materials Chemistry B, 2021, 9, 2899-2908.	2.9	32
14	Recent advances in carbon dots for bioimaging applications. Nanoscale Horizons, 2020, 5, 218-234.	4.1	192
15	Revealing the relationship between the Au decoration method and the enhanced acetone sensing performance of a mesoporous In <sub>2</sub> O <sub>3</sub> -based gas sensor. Journal of Materials Chemistry C, 2020, 8, 78-88.	2.7	53
16	Insight into the effect of the continuous testing and aging on the SO2 sensing characteristics of a YSZ (Yttria-stabilized Zirconia)-based sensor utilizing ZnGa2O4 and Pt electrodes. Journal of Hazardous Materials, 2020, 388, 121772.	6.5	17
17	UV-activated ultrasensitive and fast reversible ppb NO2 sensing based on ZnO nanorod modified by constructing interfacial electric field with In2O3 nanoparticles. Sensors and Actuators B: Chemical, 2020, 305, 127498.	4.0	70
18	Mixed potential type H2S sensor based on stabilized zirconia and a Co2SnO4 sensing electrode for halitosis monitoring. Sensors and Actuators B: Chemical, 2020, 321, 128587.	4.0	23

Geyu Lu

#	Article	IF	CITATIONS
19	The DNA controllable peroxidase mimetic activity of MoS <sub>2</sub> nanosheets for constructing a robust colorimetric biosensor. Nanoscale, 2020, 12, 19420-19428.	2.8	52
20	Understanding the noble metal modifying effect on In <sub>2</sub> O <sub>3</sub> nanowires: highly sensitive and selective gas sensors for potential early screening of multiple diseases. Nanoscale Horizons, 2019, 4, 1361-1371.	4.1	69
21	Sensitive colorimetric sensor for point-of-care detection of acetylcholinesterase using cobalt oxyhydroxide nanoflakes. Journal of Materials Chemistry B, 2019, 7, 1230-1237.	2.9	50
22	A rapid-response room-temperature planar type gas sensor based on DPA-Ph-DBPzDCN for the sensitive detection of NH <sub>3</sub> . Journal of Materials Chemistry A, 2019, 7, 4744-4750.	5.2	37
23	Graphene quantum dot-functionalized three-dimensional ordered mesoporous ZnO for acetone detection toward diagnosis of diabetes. Nanoscale, 2019, 11, 11496-11504.	2.8	71
24	Realizing the Control of Electronic Energy Level Structure and Gas-Sensing Selectivity over Heteroatom-Doped In <sub>2</sub> 0 <sub>3</sub> Spheres with an Inverse Opal Microstructure. ACS Applied Materials & Interfaces, 2019, 11, 9600-9611.	4.0	76
25	High-activity Mo, S co-doped carbon quantum dot nanozyme-based cascade colorimetric biosensor for sensitive detection of cholesterol. Journal of Materials Chemistry B, 2019, 7, 7042-7051.	2.9	98
26	Ultrasensitive gas sensor based on hollow tungsten trioxide-nickel oxide (WO3-NiO) nanoflowers for fast and selective xylene detection. Journal of Colloid and Interface Science, 2019, 535, 458-468.	5.0	90
27	A highly sensitive and moisture-resistant gas sensor for diabetes diagnosis with Pt@In2O3 nanowires and a molecular sieve for protection. NPG Asia Materials, 2018, 10, 293-308.	3.8	129
28	Yellow-Emissive Carbon Dot-Based Optical Sensing Platforms: Cell Imaging and Analytical Applications for Biocatalytic Reactions. ACS Applied Materials & amp; Interfaces, 2018, 10, 7737-7744.	4.0	87
29	Rational design of 3D inverse opal heterogeneous composite microspheres as excellent visible-light-induced NO <sub>2</sub> sensors at room temperature. Nanoscale, 2018, 10, 4841-4851.	2.8	63
30	Humidity sensor based on solution processible microporous silica nanoparticles. Sensors and Actuators B: Chemical, 2018, 266, 131-138.	4.0	34
31	The room temperature gas sensor based on Polyaniline@flower-like WO3 nanocomposites and flexible PET substrate for NH3 detection. Sensors and Actuators B: Chemical, 2018, 259, 505-513.	4.0	159
32	Novel Self-Assembly Route Assisted Ultra-Fast Trace Volatile Organic Compounds Gas Sensing Based on Three-Dimensional Opal Microspheres Composites for Diabetes Diagnosis. ACS Applied Materials & Interfaces, 2018, 10, 32913-32921.	4.0	40
33	APTES-functionalized thin-walled porous WO <sub>3</sub> nanotubes for highly selective sensing of NO <sub>2</sub> in a polluted environment. Journal of Materials Chemistry A, 2018, 6, 10976-10989.	5.2	100
34	The facile synthesis of MoO <sub>3</sub> microsheets and their excellent gas-sensing performance toward triethylamine: high selectivity, excellent stability and superior repeatability. New Journal of Chemistry, 2018, 42, 15111-15120.	1.4	73
35	A fluorescent biosensor based on molybdenum disulfide nanosheets and protein aptamer for sensitive detection of carcinoembryonic antigen. Sensors and Actuators B: Chemical, 2018, 273, 185-190.	4.0	88
36	Flower-like ZnO hollow microspheres loaded with CdO nanoparticles as high performance sensing material for gas sensors. Sensors and Actuators B: Chemical, 2017, 250, 692-702.	4.0	84

Geyu Lu

#	Article	IF	CITATIONS
37	Fabrication of well-ordered porous array mounted with gold nanoparticles and enhanced sensing properties for mixed potential-type zirconia-based NH3 sensor. Sensors and Actuators B: Chemical, 2017, 243, 1083-1091.	4.0	37
38	NH3 gas sensing performance enhanced by Pt-loaded on mesoporous WO3. Sensors and Actuators B: Chemical, 2017, 238, 473-481.	4.0	181
39	High-temperature NO2 gas sensor based on stabilized zirconia and CoTa2O6 sensing electrode. Sensors and Actuators B: Chemical, 2017, 240, 148-157.	4.0	52
40	Improvement of NO <sub>2</sub> sensing characteristic for mixed potential type gas sensor based on YSZ and Rh/Co <sub>3</sub> V <sub>2</sub> O <sub>8</sub> sensing electrode. RSC Advances, 2017, 7, 49440-49445.	1.7	11
41	High-temperature stabilized zirconia-based sensors utilizing MNb2O6 (M: Co, Ni and Zn) sensing electrodes for detection of NO2. Sensors and Actuators B: Chemical, 2016, 232, 523-530.	4.0	35
42	Fabrication of Well-Ordered Three-Phase Boundary with Nanostructure Pore Array for Mixed Potential-Type Zirconia-Based NO <sub>2</sub> Sensor. ACS Applied Materials & Interfaces, 2016, 8, 16752-16760.	4.0	41
43	Mixed-potential type NO sensor using stabilized zirconia and MoO3–In2O3 nanocomposites. Ceramics International, 2016, 42, 12503-12507.	2.3	37
44	Preparation of Ag-loaded mesoporous WO3 and its enhanced NO2 sensing performance. Sensors and Actuators B: Chemical, 2016, 225, 544-552.	4.0	127
45	YSZ-based NO2 sensor utilizing hierarchical In2O3 electrode. Sensors and Actuators B: Chemical, 2016, 222, 698-706.	4.0	40
46	Ultrasensitive and low detection limit of acetone gas sensor based on W-doped NiO hierarchical nanostructure. Sensors and Actuators B: Chemical, 2015, 220, 59-67.	4.0	133
47	High performance mixed-potential type NO2 sensors based on three-dimensional TPB and Co3V2O8 sensing electrode. Sensors and Actuators B: Chemical, 2015, 216, 121-127.	4.0	40
48	Mixed-potential type NH3 sensor based on stabilized zirconia and Ni3V2O8 sensing electrode. Sensors and Actuators B: Chemical, 2015, 210, 795-802.	4.0	96
49	Highly Enhanced Sensing Properties for ZnO Nanoparticle-Decorated Round-Edged α-Fe <sub>2</sub> O <sub>3</sub> Hexahedrons. ACS Applied Materials & Interfaces, 2015, 7, 8743-8749.	4.0	62
50	Enhancement of NO2 gas sensing response based on ordered mesoporous Fe-doped In2O3. Sensors and Actuators B: Chemical, 2014, 191, 806-812.	4.0	141
51	Cu-doped α-Fe2O3 hierarchical microcubes: Synthesis and gas sensing properties. Sensors and Actuators B: Chemical, 2014, 193, 616-622.	4.0	115
52	High Performance Mixed-Potential Type NOx Sensor Based On Stabilized Zirconia and Oxide Electrode. Solid State Ionics, 2014, 262, 292-297.	1.3	51
53	Microwave hydrothermal synthesis and gas sensing application of porous ZnO core–shell microstructures. RSC Advances, 2014, 4, 32538.	1.7	36
54	Hydrothermally growth of novel hierarchical structures titanium dioxide for high efficiency dye-sensitized solar cells. Journal of Power Sources, 2014, 268, 19-24.	4.0	20

Geyu Lu

#	Article	IF	CITATIONS
55	Hierarchical α-Fe <sub>2</sub> 0 <sub>3</sub> /NiO Composites with a Hollow Structure for a Gas Sensor. ACS Applied Materials & Interfaces, 2014, 6, 12031-12037.	4.0	255
56	Hierarchical flower-like WO3 nanostructures and their gas sensing properties. Sensors and Actuators B: Chemical, 2014, 204, 224-230.	4.0	111
57	One-step synthesis and gas sensing properties of hierarchical Cd-doped SnO2 nanostructures. Sensors and Actuators B: Chemical, 2014, 190, 32-39.	4.0	122
58	The effects of sintering temperature of MnCr2O4 nanocomposite on the NO2 sensing property for YSZ-based potentiometric sensor. Sensors and Actuators B: Chemical, 2013, 177, 397-403.	4.0	73
59	Mixed-potential-type NO2 sensor using stabilized zirconia and Cr2O3–WO3 nanocomposites. Sensors and Actuators B: Chemical, 2013, 180, 90-95.	4.0	59
60	Preparation and gas sensing properties of hierarchical flower-like In2O3 microspheres. Sensors and Actuators B: Chemical, 2013, 176, 405-412.	4.0	84
61	One-step synthesis and gas sensing characteristics of urchin-like In2O3. Sensors and Actuators B: Chemical, 2013, 186, 61-66.	4.0	31
62	Gas sensing with hollow α-Fe2O3 urchin-like spheres prepared via template-free hydrothermal synthesis. CrystEngComm, 2012, 14, 8335.	1.3	38
63	UV-enhanced room temperature NO2 sensor using ZnO nanorods modified with SnO2 nanoparticles. Sensors and Actuators B: Chemical, 2012, 162, 82-88.	4.0	251
64	Ammonia sensor based on NASICON and Cr2O3 electrode. Sensors and Actuators B: Chemical, 2009, 136, 479-483.	4.0	65
65	Improved NH3, C2H5OH, and CH3COCH3 sensing properties of SnO2 nanofibers by adding block copolymer P123. Sensors and Actuators B: Chemical, 2009, 141, 174-178.	4.0	59
66	High-temperature sensors for NO and NO2 based on stabilized zirconiaand spinel-type oxide electrodes. Journal of Materials Chemistry, 1997, 7, 1445-1449.	6.7	130